

Easy-cone state mediating the spin reorientation in topological kagome magnet Fe_3Sn_2

L. Prodan,¹ D. M. Evans,^{1,2} A. S. Sukhanov,³ S. E. Nikitin,⁴ A. A. Tsirlin,⁵ L. Puntingam,¹ M. C. Rahn,³ L. Chioncel,⁶ V. Tsurkan,^{1,7} and I. Kézsmárki¹

¹*Experimentalphysik V, Center for Electronic Correlations and Magnetism,
Institute of Physics, University of Augsburg, D-86159 Augsburg, Germany*

²*Department of Sustainable Energy Technology, SINTEF Industry, Oslo, Norway*

³*Experimentalphysik VI, Center for Electronic Correlations and Magnetism,
Institute of Physics, University of Augsburg, D-86159 Augsburg, Germany*

⁴*PSI Center for Neutron and Muon Sciences,
Paul Scherrer Institut, CH-5232 Villigen-PSI, Switzerland*

⁵*Felix Bloch Institute for Solid-State Physics,
Leipzig University, D-04103 Leipzig, Germany*

⁶*Theoretische Physik III, Institute of Physics,
University of Augsburg, D-86135 Augsburg, Germany*

⁷*Institute of Applied Physics, Moldova State University, MD 2028 Chișinău, R. Moldova*

Abstract

We investigated temperature-driven spin reorientation (SR) in the itinerant kagome magnet Fe_3Sn_2 using high-resolution synchrotron x-ray diffraction, neutron diffraction, magnetometry, and magnetic force microscopy (MFM), further supported by phenomenological analysis. Our study reveals a crossover from the state with easy-plane anisotropy to the high-temperature state with uniaxial easy-axis anisotropy taking place between $\sim 40 - 130$ K through an intermediate easy-cone (or tilted spin) state. This state, induced by the interplay between the anisotropy constants K_1 and K_2 , is clearly manifested in the thermal evolution of the magnetic structure factor, which reveals a gradual change of the SR angle θ between 40 – 130 K. We also found that the SR is accompanied by a magnetoelastic effect. Zero-field MFM images across the SR range show a transformation in surface magnetic patterns from a dendritic structure at 120 K, to domain wall dominated MFM contrast at 40 K.

*To whom correspondence should be addressed. Email: lilian.prodan@uni-a.de

I. INTRODUCTION

In anisotropic magnetic materials, the easy axis of magnetization denotes the direction along which magnetic moments align, minimizing the internal energy of the system [1]. The interplay between magnetocrystalline anisotropy, dipolar, and Dzyaloshinskii-Moriya interactions (DMI) might lead to a reorientation of magnetic moments [2, 3]. The possibility of controlling magnetic degrees of freedom through the interplay between different types of interactions has been the focus of extensive studies in recent decades [4–7]. This has been extensively studied for thin films and multilayered structures where long-range magnetic dipolar interaction dominates, forcing magnetic moments to follow shape anisotropy [8]. On the other hand, in RE-TM magnets (RE = Pr, Nd, Tb, Dy, Ho; TM = Mn, Fe, Co) the competition between the anisotropies of rare-earth and transition-metal sublattices drives the so-called spin reorientation (SR) transition [9–12], where the direction of the easy axis of magnetization rotates from one crystallographic axis to another with varying the temperature. Moreover, temperature-induced changes in the local environment and magnetic interactions between ions at different Wyckoff positions due to symmetry change can also induce spin reorientation effects [13].

Depending on whether the easy axis shifts abruptly or rotates continuously between crystal symmetry axes, the reorientation is characterized as a first- or second-order phase transition, respectively, or can even be a smooth crossover [14]. A first-order magnetic transition is usually accompanied by a hysteresis in the magnetization and substantial changes in the magnetic entropy [15–17]. In contrast, second-order phase transitions can be traced as distinct anomalies in the magnetic susceptibility, while crossovers may not be accompanied by any sharp anomaly in thermodynamic quantities [15, 18, 19].

Recently, there has been growing interest in materials exhibiting SR, where the orientation of the easy axis can be influenced by a range of intrinsic and extrinsic factors, including chemical composition [20, 21], shape [8], magnetic field [22–24], external pressure [25, 26], strain [27, 28], and light [29]. These factors often involve significant changes in the magnetic and electronic properties of materials and lead to the emergence of novel quantum phenomena. In particular, in several non-centrosymmetric magnets, it has been demonstrated that the interplay between DMI and magnetic anisotropy is crucial for stabilizing topologically protected (anti)skyrmion states [5, 21, 30–36]. Lorentz force microscopy studies on

$\text{Nd}_2\text{Fe}_{14}\text{B}$ have revealed the formation of magnetic bubbles with zero topological number and magnetic skyrmions induced by SR [37]. Moreover, the enhancement of magnetoresistance, topological, and anomalous Hall effects have been reported near the SR transition in various two-dimensional van der Waals magnets [7, 38, 39], rare-earth topological kagome magnets of RMn_6Sn_6 -type [40, 41], and Heusler magnets [42]. These phenomena are attributed to changes in Berry curvature during spin reorientation [43].

Here, we investigate the SR effect in the itinerant kagome magnet Fe_3Sn_2 . The crystal structure consists of bilayers of Fe_3Sn kagome networks separated by hexagonal Sn layers and stacked along the \mathbf{c} axis [see Fig. 1(a)], corresponding to rhombohedral $R\bar{3}m$ space group [44]. Fe_3Sn_2 is ferromagnetic below 650 K and its magnetic anisotropy is reported to change from the easy-axis (EA) above 250 K to the easy-plane (EP) below 60 K [45, 46]. This material has recently attracted much attention as a host for massive Dirac fermionic states [47], Weyl nodes [48], topological flat bands [49], and helical nodal lines [50]. The interplay between the electronic band topology and magnetism gives rise to prominent phenomena, including large anomalous and topological Hall effects [47, 51], magneto-optical effects [48, 50], and topologically protected skyrmionic bubbles [52, 53]. Moreover, recent advancements in the field suggested that Fe_3Sn_2 manifests anomalous charge carrier behavior and strong orbital contribution to the magnetism and transport properties [54–57].

Despite intense studies using various measurement techniques such as magnetization, *ac*-susceptibility, neutron diffraction, magnetic force microscopy (MFM) [58–62], optical spectroscopy [48], Raman scattering [46, 61], and magnetotransport measurements [63, 64], the mechanism of spin reorientation in Fe_3Sn_2 remains unclear. Specifically, whether the transition is gradual or abrupt, its origin, and its impact on the magnetic domain configuration are still debated. Given that the electronic band topology can strongly be affected by the magnetic structure in kagome magnets, like Fe_3Sn_2 , it is essential to clarify the origin of the SR and understand the accompanying variations in spin texture with temperature and magnetic field.

In this study, we investigated the temperature-driven SR in the topological kagome ferromagnet Fe_3Sn_2 through a combination of experimental techniques and phenomenological analysis. The temperature dependence of the anisotropy constants K_1 and K_2 , the evolution of the magnetic structure factor $\mathbf{M}_{\mathbf{Q}}(T)$, and MFM imaging indicate that the high-temperature state, with uniaxial easy-axis anisotropy, transforms to a mixed state before

developing an in-plane magnetization state at low temperatures, consistent with easy-plane anisotropy. This transformation is characterized by a gradual change of the angle θ spanned by the magnetization and the **c**-axis, taking place between $\approx 40 - 130$ K. The zero-field MFM images across the SR range show strong variation in magnetic contrast. Phenomenological analysis suggests that the SR and associated microstructural transformations are the results of competing anisotropy constants K_1 and K_2 .

II. EXPERIMENTAL DETAILS

Single crystals of Fe_3Sn_2 have been grown by the chemical transport reaction method using preliminary synthesized polycrystalline material and iodine as a transport agent. The growth was carried out in a two-zone horizontal furnace in a temperature range between 670° and 740 °C. Shiny hexagonal crystals with dimensions up to 4 mm along the largest side were obtained in the hot part of the ampule. The chemical composition of the samples was checked by energy-dispersive X-ray spectroscopy (EDS) analysis utilizing the ZEISS Crossbeam 550 system.

High-resolution x-ray diffraction (XRD) data were collected on the polycrystalline sample of Fe_3Sn_2 . The measurements were performed in the transmission geometry at the ID22 beamline at the European Synchrotron Radiation Facility (ESRF, Grenoble, France) using the multianalyzer setup [65, 66]. The wavelength of 0.354217 Å was calibrated with a silicon standard (NIST, 640c). The sample temperature was stabilized with the liquid helium-cooled cryostat. To reduce the effect of beam heating, the capillary was kept open at one end and exposed to the helium-flow atmosphere. The Rietveld refinement was performed using the JANA2006 program [67].

Magnetic properties were studied with the SQUID magnetometer (MPMS 3, Quantum Design) in the temperature range of 2 – 400 K and magnetic fields up to 7 T.

Neutron diffraction data were collected on the EIGER triple axis instrument (PSI, Switzerland) with a neutron wavelength of 2.36 Å [68]. A few single crystals were coaligned to increase the total sample mass. The backscattering Laue x-ray showed that the relative misalignment between the individual crystals does not exceed 1 deg. The sample was inserted into the cryostat by its vertical [001] axis, placing the reciprocal (*HHL*) plane in the horizontal scattering plane. Graphite filter was placed after the sample to suppress the

higher-order harmonics.

To investigate the magnetic domain textures of Fe_3Sn_2 , we perform MFM on an attocube attoAFM I, equipped with a superconducting magnet, and cooled by liquid Helium cryostat. The sample environment has ca. 150 mbar of He as an exchange gas. PPP-MFMR nanosensor probes were used; these have a hard magnetic coating and a radius of curvature of ≤ 50 nm. Once each temperature was reached, the equipment was allowed to thermalize for about an hour to ensure full thermal equilibrium. Data were collected in single pass with the tip lifted 200 nm above the defined contact point, and the pixel size is 20 nm. The images show changes in frequency, recorded via a phase-sensitive feedback loop, and, as usual, the image contrast is proportional to the gradient of the stray magnetic field at the tip [69].

III. RESULTS AND DISCUSSION

Figures 1(b) and (c) show the structural parameters derived from the Rietveld refinement of the XRD data between 300 K and 10 K. The cell parameter **a** decreases by $\sim 3\%$, while **c** decreases by $\sim 2\%$ [see Fig. 1(b)]. Both parameters exhibit a change in the slope below 120 K, which is also reflected in the temperature evolution of the **c/a** ratio and the unit-cell volume, Figure 1(c), indicating a magnetoelastic response to the spin reorientation. Importantly, the reflection width changes only marginally between 300 and 10 K, and none of the reflections splits on cooling [see Figs. 1(d)-(e)]. Therefore, no deviation from the trigonal symmetry is observed down to the lowest measured temperatures.

Figures 2(a) and (b) show the isothermal magnetization curves of Fe_3Sn_2 measured for magnetic fields applied in different orientations: within the **ab** plane, along the **a** axis (in-plane), and along the **c** axis (out-of-plane). At 2 K, full saturation of magnetization M_s along the **a** axis is achieved in fields ~ 0.1 T, while along **c** axis, the saturation requires approx. 1 T. The \mathbf{M}_s calculated at 5 T are $2.09 \mu_B/\text{Fe}$ and $2.17 \mu_B/\text{Fe}$ for $\mathbf{H} \parallel \mathbf{a}$ and $\mathbf{H} \parallel \mathbf{c}$, respectively. With increasing temperature, the saturation field increases for $\mathbf{H} \parallel \mathbf{a}$ and decreases for $\mathbf{H} \parallel \mathbf{c}$. The initial susceptibility extracted from fields close to zero, χ'_0 , measured for $\mathbf{H} \parallel \mathbf{a}$ and $\mathbf{H} \parallel \mathbf{c}$ is shown in Figure 2(c).

The temperature-dependent magnetization for $\mathbf{H} \parallel \mathbf{a}$ was measured in various fields and cooling protocols. Figure 2(d) shows a continuous increase of magnetization as the temperature decreases to 60 K, saturating below this temperature. Unlike the findings in Ref. [60],

our data show gradual variation with temperature without abrupt changes between 400 K and 2 K. The zero field-cooled magnetization (ZFC) and field-cooled magnetization (FC) measurements display only minor hysteresis, which can be likely attributed to the dynamics of magnetic microstructures described later.

Next, we discuss the uniaxial crystal anisotropy energy density (E_A) that for hexagonal system is usually expressed as a power series of the form [70]:

$$E_A = \sum_n K_n \sin^{2n} \theta . \quad (1)$$

Here, K_n is the uniaxial anisotropy constant of order n and θ is the angle between M and the **c** axis. In most cases, it is sufficient to consider only the first two terms:

$$E_A = K_0 + K_1 \sin^2 \theta + K_2 \sin^4 \theta + \dots \quad (2)$$

The anisotropy energy minimization in the presence of an external applied field provides the equilibrium direction of magnetization. In the limit of zero external field, the total anisotropy energy is $K_u \approx K_1 + K_2$. This K_u constant can be estimated directly from the experimental data as the difference between the energy necessary to saturate the magnetization along the two orthogonal directions:

Figure 2(e) presents the temperature dependence of E_a and E_c used to calculate the uniaxial anisotropy constant K_u . Here, the magnetization was corrected for the demagnetization coefficient, $H_i = H - DM$, where H is the applied external magnetic field, D represents the demagnetization coefficient, and M is the magnetization. E_a decreases with a decrease in temperature, while E_c increases, reflecting the change of the anisotropy. At 120 K, the integrals have equal values, indicating that the same energy is required to align the magnetic moment along the **a** or **c** axes. Consequently, $K_u = 0$ at this temperature [see Fig. 3(a)]. At temperatures below 120 K, K_u is negative, reaching -45 kJ/m³ at 2 K, while above is positive and reaches 57 kJ/m³ at 400 K.

Figure 3(a) shows the temperature dependence of the anisotropy constants K_u , K_1 , and K_2 . In the temperature range where the orientation of moments is well-defined, we also calculated K_1 and K_2 independently by the Sucksmith-Thompson (S-T) method fitting the S-T isotherms $M/H = f(M^2)$ [73]. At 2 K, K_1 is negative (easy-plane anisotropy) and reaches ~ -75 kJ/m³ [see Figure 3(a)]. At high temperatures, K_1 is positive (easy-axis anisotropy) and reaches ~ 55 kJ/m³ at 400 K. In contrast, K_2 remains positive throughout

the whole temperature range. At 2 K, K_2 has a value ~ 30 kJ/m³. At the intermediate temperatures, 50 K \leq T \leq 150 K, the S-T isotherms show strong nonlinearity and this method gives non-reliable values anisotropy constants.

In the following, we present a new approach for extracting anisotropy constants when the S-T isotherms become nonlinear. The minimization of magnetic free energy described in Eq. 1, with respect to the reorientation angle θ (being the order parameter), gives the equilibrium configuration. In this case, the relation between the zero-field differential susceptibility for $\mathbf{H}||\mathbf{c}$ and the anisotropy constants, the saturation magnetization for $\mathbf{H}||\mathbf{c}$, and the demagnetization has the following form (see Appendix):

$$\chi(T) = \frac{M_s^2(T)}{D M_s^2(T) - 2(K_1 + 2K_2)} \quad (3)$$

The resulting temperature dependence of K_1 and K_2 is shown in Figure 3(a). Below 50 K, the values of K_1 and K_2 agree well with those obtained by the S-T method, corroborating the data obtained through the new approach.

The interplay between K_1 and K_2 controls the transition from the easy axis (EA) to the easy plane (EP) via the easy-cone (EC) state [71]. In the EC state, the easy direction of the magnetization is tilted away both from the hexagonal axis and the hexagonal plane, i.e. $0 < \theta < 90^\circ$. When the anisotropy in the hexagonal plane is negligible, the easy axes lie on the surface of a cone. In the EC state, the rotation angle is defined by $\theta(T) = \arcsin \sqrt{-K_1/2K_2}$ [11].

The temperature dependence of θ calculated from the anisotropy constants K_1 and K_2 is shown in Figure 3(b). The transition from EP to EC takes place at $T_{SR1} \approx 40$ K, when condition $-K_1 = 2K_2$ is satisfied. Upon heating in the easy-cone state, the magnetic moments rotate gradually from the **a** axis towards the **c** axis. At $T_{SR2} \approx 130$ K, K_1 changes sign, defining the transition to the easy-axis state.

The angle of SR was additionally calculated from the ratio of low-field magnetization for $\mathbf{H}||\mathbf{a}$ and $\mathbf{H}||\mathbf{c}$ for internal magnetic field $H_i=5$ Oe using the relation $\theta' = \arctan(M_a/M_c)$ [see Figure 2(f)]. The calculated θ' also shows gradual decrease with increasing temperature, being in qualitative agreement with the results using anisotropy constants.

For an independent quantification of the SR angle, we performed single-crystal neutron diffraction experiments. According to the neutron polarization factor, the scattering

intensity vanishes when the neutron momentum transfer \mathbf{Q} aligns with the magnetic structure factor $\mathbf{M}_\mathbf{Q}$. Therefore, it is convenient to track the in-plane projection of the spin upon its canting by the intensity of the allowed Bragg peaks of the indexes $(00L)$, where $L = 3, 6, 9, \dots, 3n$. Indeed, when the spins are strictly oriented along the \mathbf{c} axis, the $(00L)$ peaks contain only the nuclear intensity and no magnetic contribution. As soon as the spins deviate from the \mathbf{c} axis, the $\mathbf{Q} \parallel \mathbf{M}_\mathbf{Q}$ condition is no longer fulfilled, and a finite magnetic intensity $\propto S_{ab}$ appears on top of the nuclear Bragg peaks.

Figure 4(a) shows the intensity of the Bragg peak $[003]$ collected by rotating the crystal around its $[001]$ at a fixed detector angle $2\theta = 41.21^\circ$ (rocking scan). As can be seen, the measurements reveal almost identical Bragg peaks at 285 K and 135 K, whereas the peak intensity significantly increases at a lower temperature of 5 K. To analyze its temperature evolution, we plotted the total intensity integrated over the rocking angle of the $[003]$ peak in Fig. 4(b). The flat curve from room temperature down to ~ 130 K suggests the spins remain along the c axis and only the temperature-independent nuclear intensity is recorded. Below this temperature, the intensity shows a gradual increase over a wide temperature range down to ~ 40 K, after which it saturates. Assuming that the spins are fully in-plane at the lowest temperature, we can follow the temperature dependence of the SR by the θ angle ($\theta = 0$ when $\mathbf{M} \parallel c$) estimated from neutron diffraction, as shown in the inset of Fig. 4(b). This rotation of magnetic moments from the \mathbf{c} axis to the \mathbf{a} axis should lower the symmetry by breaking the three-fold rotational symmetry for any $\theta > 0$. The fact that the symmetry lowering from the trigonal state to an orthorhombic state has not been observed by our high-resolution x-ray study may be due to a) the weakness of the corresponding distortion and/or b) the restoring of the trigonal symmetry in macroscopic sense due to the coexistence of the energetically equivalent six domains of the EP state.

For an independent confirmation of the SR in our Fe_3Sn_2 single crystals, the magnetic domain pattern were imaged by MFM in zero field on the as-grown \mathbf{ab} plane of the crystal shown in the inset of Figure 2(f). Figure 5(a) shows the MFM pattern at 120 K, revealing a dendrite-like fern contrast. This is similar to the domain pattern at 300 K which previous work showed arises from magnetization pointing upward and downward along the \mathbf{c} axis, see e.g. Refs. [53, 59, 60]. We note that the fern pattern is caused by surface branching of the underlying domains, and therefore the domain patterns observed here with MFM in Fe_3Sn_2 do not reflect the magnetic microstructure in the bulk. Indeed, such dendrite-like

domain patterns have been reported to be characteristic of uniaxial easy-axis magnets [74]. With cooling down to 80 K, where the magnetic easy axis is already tilted away from the c axis according to our magnetometry and neutron diffraction results, the MFM contrast undergoes gradual changes, namely the dendrite-like structure transforms to a more simple stripe domain pattern. Similar transformation of magnetic domains in Fe_3Sn_2 thin plates was reported to result from tilting of spins away from the c axis [75]. With further cooling to 40 K the stripe pattern vanishes. In fact, in Figure 5(c) the magnetic contrast caused by out-of-plane stray fields disappears, indicating that the sample becomes in-plane magnetized. In that case, vortices and antivortices (also termed in-plane flux closure domains) are expected to form, as shown for the easy-plane ferromagnet Fe_3Sn [72]. These results are qualitatively in agreement with MFM results reported in Refs. [60, 62] and clearly demonstrate the onset of a SR from a high-temperature easy-axis state to a low-temperature easy-plane state.

A quantitative analysis of the magnetic behavior at the micrometer-length scale is usually obtained by micromagnetic simulations, which can provide a comprehensive description of MFM images. In combination with density functional theory, these simulations can consider various forms of exchange interactions and anisotropies. While here we focus on the analysis of the temperature-dependent SR process, MFM imaging is only used to provide another independent confirmation of the SR. A multi-scale approach reproducing the magnetic patterns observed in zero as well as finite magnetic fields will be presented in a forthcoming work.

IV. CONCLUSION

In conclusion, we have investigated the temperature-driven spin reorientation in the topological kagome ferromagnet Fe_3Sn_2 by high-resolution synchrotron x-ray diffraction, magnetometry, neutron diffraction, and MFM techniques supported by phenomenological analysis of magnetic anisotropy. Our study reveals an intermediate easy-cone state that appears during the reorientation from the easy-plane towards the easy-axis state. Although spin reorientation is accompanied by a weak magnetoelastic effect, no lowering of the crystal symmetry from trigonal was resolved down to the lowest temperatures. The temperature dependence of the first- and second-order anisotropy constants, K_1 and K_2 , and the evolution of the magnetic structure factor $\mathbf{M}_\mathbf{Q}(T)$ show that the easy-cone state is stable between $T_{SR1} \approx 40$ K

and $T_{SR2} \approx 130$ K. The spin reorientation angle θ , determined from the magnetometry and neutron diffraction data, exhibits a gradual change between T_{SR1} and T_{SR2} . Furthermore, zero-field MFM images across the SR range evidence a transformation in magnetic contrast, from a dendritic structure at 120 K to well-defined domain walls at 40 K, providing a direct visualization of spin reorientation in Fe_3Sn_2 . Our phenomenological analysis highlights the dominant role of competition between anisotropy constants. These findings provide a clear insight into the nature and dynamics of spin reorientation in topological magnet Fe_3Sn_2 , highlighting its fundamental role in the evolution of magnetic anisotropy.

ACKNOWLEDGMENTS

We thank ESRF for providing the beamtime for the project HC-4369 and acknowledge Ola Grendal as well as Andrew Fitch for their technical support at ID22. This work was supported by the Deutsche Forschungsgemeinschaft (DFG, German Research Foundation) – TRR 360 – 492547816. D.M.E. acknowledges and thank the DFG for financial support via DFG individual fellowship number EV 305/1-1. VT acknowledges support through project ANCD (code 011201, Moldova).

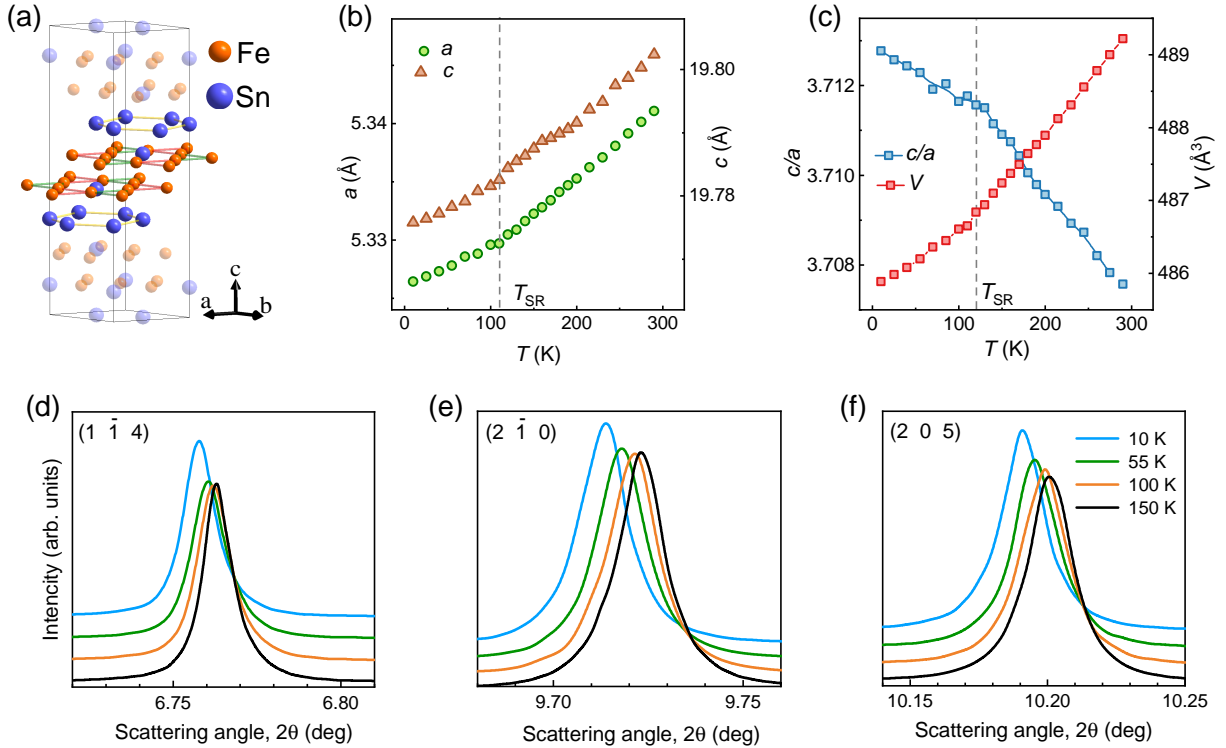


FIG. 1. Crystal structure and high-resolution powder X-ray synchrotron diffraction for Fe_3Sn_2 . (a) Schematic representation of the rhombohedral $R\bar{3}m$ crystal structure [44]. (b) Temperature dependence of the lattice parameters **a** and **c**. (c) Temperature variation of the ratio **c/a** and the unit-cell volume. The vertical dashed lines in (b) and (c) indicate the changes in the slope at the spin-reorientation temperature, T_{SR} . (d)-(f) Experimental profiles of the $(1\bar{1}4)$, $(2\bar{1}0)$, and (205) Bragg reflections as measured at different temperatures by high-resolution synchrotron powder XRD. The same color code is used in panels (d-f).

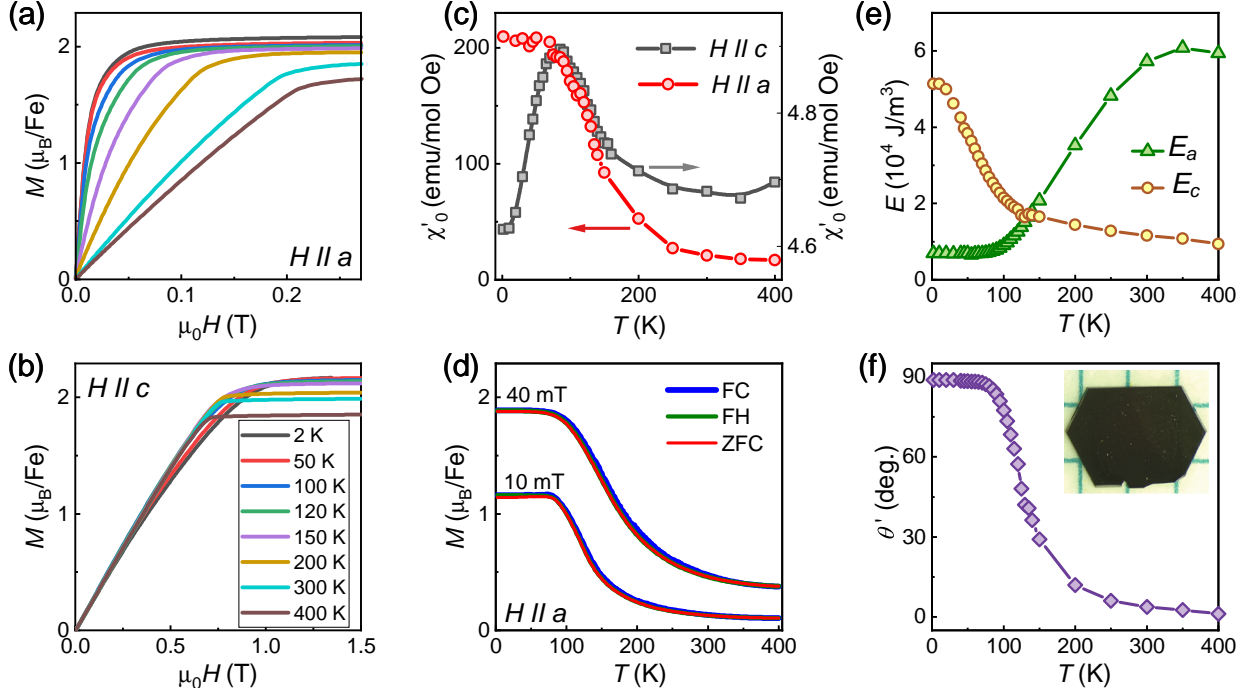


FIG. 2. SQUID magnetometry data of ferromagnetic Fe_3Sn_2 . (a) Magnetization curves *vs* magnetic field applied along the **a** axis and (b) along the **c** axis, respectively. (c) Temperature dependence of differential magnetic susceptibility extracted from zero magnetic field measurements for $\mathbf{H} \parallel \mathbf{a}$ and $\mathbf{H} \parallel \mathbf{c}$. (d) Zero-field-cooled (ZFC), field-cooled (FC), and field-heated (FH) magnetization as a function of the temperature measured in fields of 10 and 40 mT applied along the **a** axis. (e) The temperature dependence of energy of magnetization for E_a and E_c used for calculating the uniaxial anisotropy constant K_u . (f) The temperature dependence of spin reorientation angle θ' calculated from the magnetization in $H_i = 5 \text{ Oe}$. The inset of (f) includes an optical image of the **ab** plane of the as-grown Fe_3Sn_2 crystal on a mm scale.

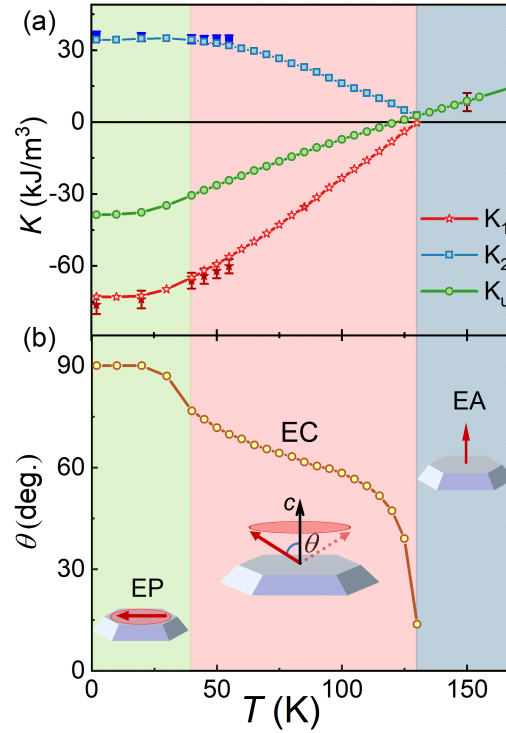


FIG. 3. (a) Temperature dependence of the anisotropy constants K_u , K_1 and K_2 obtained by the area method and eq.3 (open symbols). The closed symbols show K_1 and K_2 obtained by the Sucksmith-Thompson method. (b) Temperature dependence of the spin reorientation angle θ , as calculated using K_1 and K_2 . The insets show schematically the spin arrangement in easy-plane (EP), easy-cone (EC), and easy-axis states (EA).

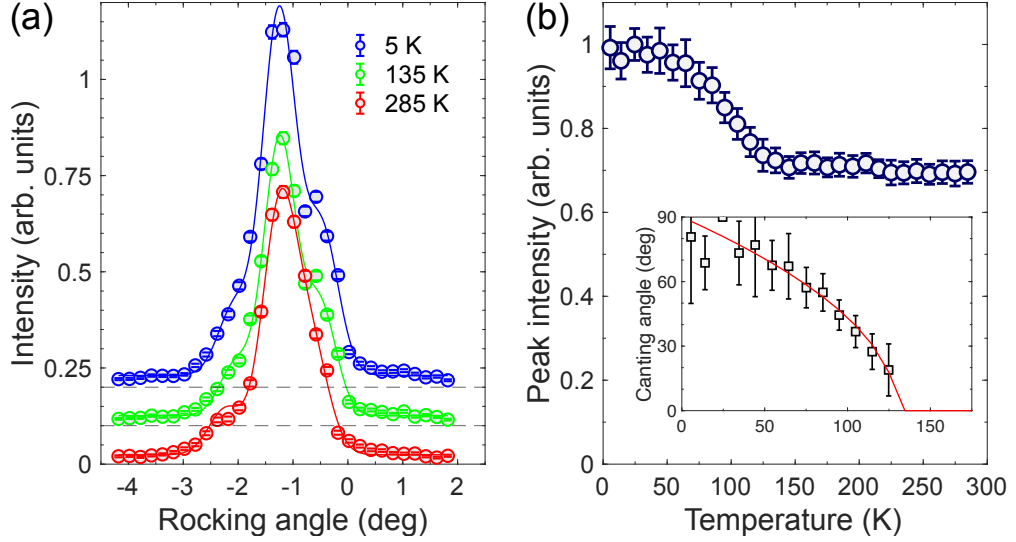


FIG. 4. Neutron diffraction: (a) The rocking-scan intensity of the (003) Bragg peak at different temperatures. The data were offset for clarity by the dashed lines. (b) The temperature dependence of the integrated intensity (area) of the (003) Bragg peak. The inset shows the calculated spin reorientation angle θ . The red curve is a guide to an eye.

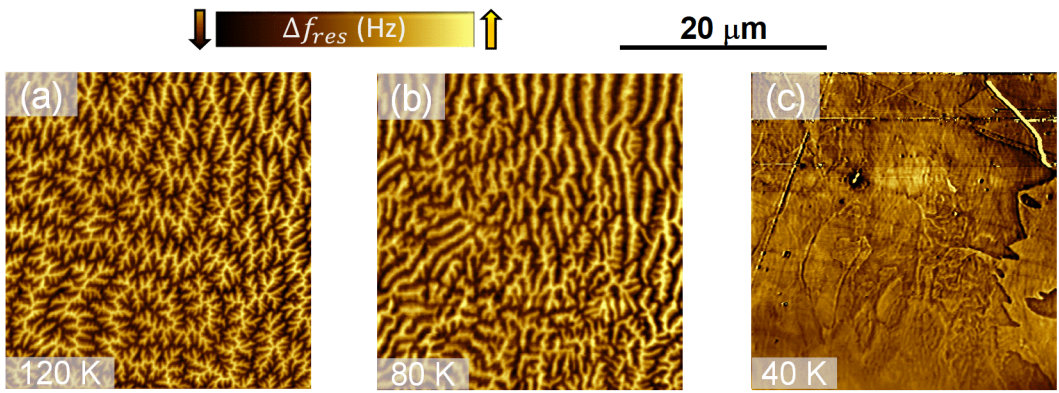


FIG. 5. Evolution of the magnetic domain patterns illustrated using MFM contrasts. Image (a) shows dendrite-like domains with out-of-plane component of magnetization measured at 120 K. Panel (b) shows a stripe domain pattern forming at 80 K. Panel (c) illustrates the lack of out-of-plane contrast at 40 K.

Appendix A: The formula of differential susceptibility

In the following we present a brief description of the derivation of Eq. (3). To simplify formulas, we introduce the reduced parameters: $k = K_1/K_2$, $A = M_s H/K_2$, $B = DM_s^2/(2K_2)$. The free energy is a functional of applied field and temperature and contains besides the Zeeman term the demagnetization energy contribution:

$$E[k, A, B] = \frac{E - K_0}{K_2} = k \sin^2 \theta + \sin^4 \theta - A \cos \theta + B \cos^2 \theta \quad (\text{A1})$$

The substitution with a variable $\gamma = \cos \theta = M_{||}/M_s$, leads the free energy into a fourth-order expression in γ . The equilibrium configuration for the orientation of the magnetic moments is found by minimization with respect to the reorientation angle $\theta = \text{Arccos } \gamma$. Conventionally, this angle is measured with respect to the c axis. The partial derivative with respect to γ : $\partial E[k, A, B]/\partial \gamma = 0$, therefore, produces a third-order equation that is analytically solvable. Two of its complex solutions are discarded, and the real solution has an analytical form:

$$\gamma = \frac{\left(432A + \sqrt{186624A^2 + 4(-48 + 24B - 24k)^3}\right)^{1/3}}{12 \cdot 2^{1/3}} - \frac{-48 + 24B - 24k}{6 \cdot 2^{2/3} \left(432A + \sqrt{186624A^2 + 4(-48 + 24B - 24k)^3}\right)^{1/3}} \quad (\text{A2})$$

The above equation represents in fact the reduced magnetization $M_{||}/M_s$, with $M_{||}$ being the magnetization along the applied field and M_s the saturated magnetization (as described in the main text). Accordingly, the differential susceptibility is computed as a derivative of magnetization with respect to the applied field:

$$\chi(H, T) = \frac{dM_{||}}{dH} = \frac{M_s^2}{K_2} \frac{d\gamma}{dA}$$

Within the reduced variables taking the derivative with respect to the variable A : $d\gamma/dA$, finally the limit $A \rightarrow 0$ gives:

$$\chi(k, A, B)|_{A \rightarrow 0} = \frac{M_s^2}{K_2} \frac{1}{2(-2 + B - k)} \quad (\text{A3})$$

Inserting back the forms of the reduced variables B and k leads to the form presented as Eq. (3).

- [1] K.H.J. Buschow and F.R. de Boer, *Physics of Magnetism and Magnetic Materials*, 1st ed. (Kluwer Academic Publishers, New York, NY, 2004).
- [2] I. Dzyaloshinsky, “A thermodynamic theory of “weak” ferromagnetism of antiferromagnetics,” *Journal of Physics and Chemistry of Solids* **4**, 241–255 (1958).
- [3] Tôru Moriya, “Anisotropic Superexchange Interaction and Weak Ferromagnetism,” *Physical Review* **120**, 91–98 (1960).
- [4] N. Locatelli, V. Cros, and J. Grollier, “Spin-torque building blocks,” *Nature Materials* **13**, 11–20 (2013).
- [5] Shulan Zuo, Jun Liu, Kaiming Qiao, Ying Zhang, Jie Chen, Na Su, Yanli Liu, Jun Cao, Tongyun Zhao, Jingmin Wang, Fengxia Hu, Jirong Sun, Chengbao Jiang, and Baogen Shen, “Spontaneous Topological Magnetic Transitions in NdCo₅ Rare-Earth Magnets,” *Advanced Materials* **33** (2021), 10.1002/adma.202103751.
- [6] Virna Kisiček, Damir Dominko, Matija Čulo, Željko Rapljenović, Marko Kuveždić, Martina Dragičević, Helmuth Berger, Xavier Rocquefelte, Mirta Herak, and Tomislav Ivec, “Spin-Reorientation-Driven Linear Magnetoelectric Effect in Topological Antiferromagnet Cu₃TeO₆,” *Phys. Rev. Lett.* **132**, 096701 (2024).
- [7] Riju Pal, Buddhadeb Pal, Suchanda Mondal, Rajesh O. Sharma, Tanmoy Das, Prabhat Mandal, and Atindra Nath Pal, “Spin-reorientation driven emergent phases and unconventional magnetotransport in quasi-2D vdW ferromagnet Fe₄GeTe₂,” *npj 2D Materials and Applications* **8** (2024), 10.1038/s41699-024-00463-y.
- [8] M. T. Johnson, P. J. H. Bloemen, F. J. A. den Broeder, and J. J. de Vries, “Magnetic anisotropy in metallic multilayers,” *Reports on Progress in Physics* **59**, 1409–1458 (1996).
- [9] R. L. White, “Review of recent work on the magnetic and spectroscopic properties of the rare-earth orthoferrites,” *Journal of Applied Physics* **40**, 1061–1069 (1969).
- [10] T. Yamaguchi, “Theory of spin reorientation in rare-earth orthochromites and orthoferrites,” *Journal of Physics and Chemistry of Solids* **35**, 479–500 (1974).
- [11] P.A. Algarabel, A.del Moral, M.R. Ibarra, and J.I. Arnaudas, “Spin reorientation in RECo₅ compounds: A.C. susceptibility and thermal expansion,” *Journal of Physics and Chemistry of Solids* **49**, 213–222 (1988).

[12] Zhentao Huang, Wei Wang, Huiqing Ye, Song Bao, Yanyan Shangguan, Junbo Liao, Saizheng Cao, Ryoichi Kajimoto, Kazuhiko Ikeuchi, Guochu Deng, Michael Smidman, Yu Song, Shun-Li Yu, Jian-Xin Li, and Jinsheng Wen, “Microscopic origin of the spin-reorientation transition in the kagome topological magnet TbMn_6Sn_6 ,” *Physical Review B* **109**, 014434 (2024).

[13] Mads C. Weber, Mael Guennou, Donald M. Evans, Constance Toulouse, Arkadiy Simonov, Yevheniia Kholina, Xiaoxuan Ma, Wei Ren, Shixun Cao, Michael A. Carpenter, Brahim Dkhil, Manfred Fiebig, and Jens Kreisel, “Emerging spin–phonon coupling through cross-talk of two magnetic sublattices,” *Nature Communications* **13** (2022), 10.1038/s41467-021-27267-8.

[14] Lionel M. Levinson, Marshall Luban, and S. Shtrikman, “Microscopic Model for Reorientation of the Easy Axis of Magnetization,” *Physical Review* **187**, 715–722 (1969).

[15] Konstantin P Belov, Anatolii K Zvezdin, Antonina M Kadomtseva, and R Z Levitin, “Spin-reorientation transitions in rare-earth magnets,” *Soviet Physics Uspekhi* **19**, 574–596 (1976).

[16] S. J. Yuan, Y. M. Cao, L. Li, T. F. Qi, S. X. Cao, J. C. Zhang, L. E. DeLong, and G. Cao, “First-order spin reorientation transition and specific-heat anomaly in CeFeO_3 ,” *Journal of Applied Physics* **114** (2013), 10.1063/1.4821516.

[17] Yuzhu Song, Jimin Zhang, Hengchao Li, Hong Zhong, Feixiang Long, Zhan Wang, Yuanji Xu, Xinqi Zheng, Hu Zhang, Qingzhen Huang, Ying Zhang, Xianran Xing, and Jun Chen, “Unusual Magnetocaloric Effect Triggered by Spin Reorientation,” *Advanced Energy Materials* (2024), 10.1002/aenm.202402527.

[18] Jia Yan Law, Victorino Franco, Luis Miguel Moreno-Ramírez, Alejandro Conde, Dmitriy Y. Karpenkov, Iliya Radulov, Konstantin P. Skokov, and Oliver Gutfleisch, “A quantitative criterion for determining the order of magnetic phase transitions using the magnetocaloric effect,” *Nature Communications* **9** (2018), 10.1038/s41467-018-05111-w.

[19] H. Horner and C. M. Varma, “Nature of Spin-Reorientation Transitions,” *Physical Review Letters* **20**, 845–846 (1968).

[20] Robert G. Moore, Satoshi Okamoto, Haoxiang Li, William R. Meier, Hu Miao, Ho Nyung Lee, Makoto Hashimoto, Donghui Lu, Elbio Dagotto, Michael A. McGuire, and Brian C. Sales, “Topological electronic structure evolution with symmetry-breaking spin reorientation in $(\text{Fe}_{1-x}\text{Co}_x)\text{Sn}$,” *Physical Review B* **106**, 115141 (2022).

[21] Kosuke Karube, Licong Peng, Jan Masell, Mamoun Hemmida, Hans-Albrecht Krug von Nidda, István Kézsmárki, Xiuzhen Yu, Yoshinori Tokura, and Yasujiro Taguchi, “Doping Control of

Magnetic Anisotropy for Stable Antiskyrmion Formation in Schreibersite $(\text{Fe},\text{Ni})_3\text{P}$ with S4 symmetry,” Advanced Materials **34** (2022), 10.1002/adma.202108770.

[22] H. Masuda, H. Sakai, H. Takahashi, Y. Yamasaki, A. Nakao, T. Moyoshi, H. Nakao, Y. Murakami, T. Arima, and S. Ishiwata, “Field-induced spin reorientation in the antiferromagnetic Dirac material EuMnBi_2 revealed by neutron and resonant x-ray diffraction,” Physical Review B **101**, 174411 (2020).

[23] Sh. Yamamoto, H. Suwa, T. Kihara, T. Nomura, Y. Kotani, T. Nakamura, Y. Skourski, S. Zherlitsyn, L. Prodan, V. Tsurkan, H. Nojiri, A. Loidl, and J. Wosnitza, “Element-specific field-induced spin reorientation and tetracritical point in MnCr_2S_4 ,” Physical Review B **103**, l020408 (2021).

[24] L. Prodan, S. Yasin, A. Jesche, J. Deisenhofer, H.-A. Krug von Nidda, F. Mayr, S. Zherlitsyn, J. Wosnitza, A. Loidl, and V. Tsurkan, “Unusual field-induced spin reorientation in FeCr_2S_4 : Field tuning of the Jahn-Teller state,” Physical Review B **104**, l020410 (2021).

[25] Zhisheng Lin, Mark Lohmann, Zulfikhar A. Ali, Chi Tang, Junxue Li, Wenyu Xing, Jiangnan Zhong, Shuang Jia, Wei Han, Sinisa Coh, Ward Beyermann, and Jing Shi, “Pressure-induced spin reorientation transition in layered ferromagnetic insulator $\text{Cr}_2\text{Ge}_2\text{Te}_6$,” Physical Review Materials **2**, 051004 (2018).

[26] S. A. Skorobogatov, L. S. Wu, T. Xie, K. A. Shaykhutdinov, E. V. Pomjakushina, A. Podlesnyak, and S. E. Nikitin, “Pressure control of the spin reorientation transition in the rare-earth orthoferrite YbFeO_3 ,” Physical Review B **108**, 054432 (2023).

[27] C. Bordel, J. Juraszek, David W. Cooke, C. Baldasseroni, S. Mankovsky, J. Minár, H. Ebert, S. Moyerman, E. E. Fullerton, and F. Hellman, “Fe Spin Reorientation across the Metamagnetic Transition in Strained FeRh Thin Films,” Physical Review Letters **109**, 117201 (2012).

[28] D. Kong, A. Kovács, M. Charilaou, M. Altthaler, L. Prodan, V. Tsuran, D. Meier, X. Han, I. Kezsmárki, and R. E. Dunin-Borkowski, “Strain engineering of magnetic anisotropy in the kagome magnet Fe_3Sn_2 ,” (2024).

[29] A. V. Kimel, A. Kirilyuk, A. Tsvetkov, R. V. Pisarev, and Th. Rasing, “Laser-induced ultrafast spin reorientation in the antiferromagnet TmFeO_3 ,” Nature **429**, 850–853 (2004).

[30] I. Kézsmárki, S. Bordács, P. Milde, E. Neuber, L. M. Eng, J. S. White, H. M. Rønnow, C. D. Dewhurst, M. Mochizuki, K. Yanai, H. Nakamura, D. Ehlers, V. Tsurkan, and A. Loidl, “Néel-type skyrmion lattice with confined orientation in the polar magnetic semiconductor GaV_4S_8 ,”

Nature Materials **14**, 1116–1122 (2015).

[31] D. Ehlers, I. Stasinopoulos, V. Tsurkan, H.-A. Krug von Nidda, T. Fehér, A. Leonov, I. Kézsmárki, D. Grundler, and A. Loidl, “Skyrmion dynamics under uniaxial anisotropy,” Physical Review B **94**, 014406 (2016).

[32] S. Bordács, A. Butykai, B. G. Szigeti, J. S. White, R. Cubitt, A. O. Leonov, S. Widmann, D. Ehlers, H.-A. Krug von Nidda, V. Tsurkan, A. Loidl, and I. Kézsmárki, “Equilibrium Skyrmion Lattice Ground State in a Polar Easy-plane Magnet,” Scientific Reports **7** (2017), 10.1038/s41598-017-07996-x.

[33] A. O. Leonov and I. Kézsmárki, “Skyrmion robustness in noncentrosymmetric magnets with axial symmetry: The role of anisotropy and tilted magnetic fields,” Physical Review B **96**, 214413 (2017).

[34] M. Preißinger, K. Karube, D. Ehlers, B. Szigeti, H.-A. Krug von Nidda, J. S. White, V. Ukleev, H. M. Rønnow, Y. Tokunaga, A. Kikkawa, Y. Tokura, Y. Taguchi, and I. Kézsmárki, “Vital role of magnetocrystalline anisotropy in cubic chiral skyrmion hosts,” npj Quantum Materials **6** (2021), 10.1038/s41535-021-00365-y.

[35] O. Meshcheriakova, S. Chadov, A. K. Nayak, U. K. Rößler, J. Kübler, G. André, A. A. Tsirlin, J. Kiss, S. Hausdorf, A. Kalache, W. Schnelle, M. Nicklas, and C. Felser, “Large Noncollinearity and Spin Reorientation in the Novel Mn₂RhSn Heusler Magnet,” Physical Review Letters **113**, 087203 (2014).

[36] A. S. Sukhanov, B. E. Zuniga Cespedes, P. Vir, A. S. Cameron, A. Heinemann, N. Martin, G. Chaboussant, V. Kumar, P. Milde, L. M. Eng, C. Felser, and D. S. Inosov, “Anisotropic fractal magnetic domain pattern in bulk Mn_{1.4}PtSn,” Physical Review B **102**, 174447 (2020).

[37] Y. Xiao, F. J. Morvan, A. N. He, M. K. Wang, H. B. Luo, R. B. Jiao, W. X. Xia, G. P. Zhao, and J. P. Liu, “Spin-reorientation transition induced magnetic skyrmion in Nd₂Fe₁₄B magnet,” Applied Physics Letters **117** (2020), 10.1063/5.0022270.

[38] Satyabrata Bera, Suman Kalyan Pradhan, Md Salman Khan, Riju Pal, Buddhadeb Pal, Sk Kalimuddin, Arnab Bera, Biswajit Das, Atindra Nath Pal, and Mintu Mondal, “Unraveling the nature of spin reorientation transition in quasi-2D vdW magnetic material, Fe₄GeTe₂,” Journal of Magnetism and Magnetic Materials **565**, 170257 (2023).

[39] Shasha Wang, Zhou Wang, Jialiang Jiang, Ying Zhang, Ruimin Li, Yan Feng, Ping Liu, Yalin Lu, Zhigao Sheng, Haifeng Du, Nan Gao, and Bin Xiang, “Temperature-driven spin

reorientation transition in van der Waals $\text{Cr}_{1.7}\text{Te}_2$ ferromagnet,” *Applied Physics Letters* **124** (2024), 10.1063/5.0202429.

[40] D. Connor Jones, Suvadip Das, Hari Bhandari, Xiaoxiong Liu, Peter Siegfried, Madhav P. Ghimire, Stepan S. Tsirkin, I. I. Mazin, and Nirmal J. Ghimire, “Origin of spin reorientation and intrinsic anomalous Hall effect in the kagome ferrimagnet TbMn_6Sn_6 ,” *Physical Review B* **110**, 115134 (2024).

[41] Bodong Lv, Rui Zhong, Xiaohua Luo, Shengcan Ma, Changcai Chen, Sujuan Wang, Qing Luo, Fei Gao, Chunsheng Fang, and Weijun Ren, “Anomalous Hall effect and topological Hall effect in Kagome lattice material $\text{Yb}_{0.90}\text{Mn}_6\text{Ge}_{3.25}\text{Ga}_{0.39}$ single crystal,” *Scripta Materialia* **255**, 116345 (2025).

[42] Vivek Kumar, Nitesh Kumar, Manfred Reehuis, Jacob Gayles, A. S. Sukhanov, Andreas Hoser, Françoise Damay, Chandra Shekhar, Peter Adler, and Claudia Felser, “Detection of antiskyrmions by topological Hall effect in Heusler compounds,” *Physical Review B* **101**, 014424 (2020).

[43] Yangkun He, Johannes Kroder, Jacob Gayles, Chenguang Fu, Yu Pan, Walter Schnelle, Claudia Felser, and Gerhard H. Fecher, “Large topological Hall effect in an easy-cone ferromagnet $(\text{Cr}_{0.9}\text{B}_{0.1})\text{Te}$,” *Applied Physics Letters* **117** (2020), 10.1063/5.0018229.

[44] B. Malaman, B. Roques, A. Courtois, and J. Protas, “Structure cristalline du stannure de fer Fe_3Sn_2 ,” *Acta Crystallographica Section B Structural Crystallography and Crystal Chemistry* **32**, 1348–1351 (1976).

[45] B. Malaman, D. Fruchart, and G. Le Caer, “Magnetic properties of Fe_3Sn_2 . II. Neutron diffraction study (and Mossbauer effect),” *Journal of Physics F: Metal Physics* **8**, 2389–2399 (1978).

[46] Ge He, Leander Peis, Ramona Stumberger, Lilian Prodan, Vladimir Tsurkan, Nico Uglert, Liviu Chioncel, István Kézsmárki, and Rudi Hackl, “Phonon Anomalies Associated with Spin Reorientation in the Kagome Ferromagnet Fe_3Sn_2 ,” *physica status solidi (b)* **259** (2021), 10.1002/pssb.202100169.

[47] Linda Ye, Mingu Kang, Junwei Liu, Felix von Cube, Christina R. Wicker, Takehito Suzuki, Chris Jozwiak, Aaron Bostwick, Eli Rotenberg, David C. Bell, Liang Fu, Riccardo Comin, and Joseph G. Checkelsky, “Massive Dirac fermions in a ferromagnetic kagome metal,” *Nature* **555**, 638–642 (2018).

[48] A. Biswas, O. Iakutkina, Q. Wang, H.C. Lei, M. Dressel, and E. Uykur, “Spin-Reorientation-

Induced Band Gap in Fe_3Sn_2 : Optical Signatures of Weyl Nodes,” Physical Review Letters **125**, 076403 (2020).

[49] Zhiyong Lin, Jin-Ho Choi, Qiang Zhang, Wei Qin, Seho Yi, Pengdong Wang, Lin Li, Yifan Wang, Hui Zhang, Zhe Sun, Laiming Wei, Shengbai Zhang, Tengfei Guo, Qingyou Lu, Jun-Hyung Cho, Changgan Zeng, and Zhenyu Zhang, “Flatbands and Emergent Ferromagnetic Ordering in Fe_3Sn_2 Kagome Lattices,” Physical Review Letters **121**, 096401 (2018).

[50] F. Schilberth, N. Uglert, L. Prodan, F. Meggle, J. Ebad Allah, C. A. Kuntscher, A. A. Tsirlin, V. Tsurkan, J. Deisenhofer, L. Chioncel, I. Kézsmárki, and S. Bordács, “Magneto-optical detection of topological contributions to the anomalous Hall effect in a kagome ferromagnet,” Phys. Rev. B **106**, 144404 (2022).

[51] Qianheng Du, Zhixiang Hu, Myung-Geun Han, Fernando Camino, Yimei Zhu, and C. Petrovic, “Topological Hall Effect Anisotropy in Kagome Bilayer Metal Fe_3Sn_2 ,” Phys. Rev. Lett. **129**, 236601 (2022).

[52] Zhipeng Hou, Weijun Ren, Bei Ding, Guizhou Xu, Yue Wang, Bing Yang, Qiang Zhang, Ying Zhang, Enke Liu, Feng Xu, Wenhong Wang, Guangheng Wu, Xixiang Zhang, Baogen Shen, and Zhidong Zhang, “Observation of various and spontaneous magnetic skyrmionic bubbles at room temperature in a frustrated kagome magnet with uniaxial magnetic anisotropy,” Adv. Mater. **30** (2018), 10.1002/adma.201706306.

[53] Markus Altthaler, Erik Lysne, Erik Roede, Lilian Prodan, Vladimir Tsurkan, Mohamed A. Kassem, Hiroyuki Nakamura, Stephan Krohns, István Kézsmárki, and Dennis Meier, “Magnetic and geometric control of spin textures in the itinerant kagome magnet Fe_3Sn_2 ,” Physical Review Research **3**, 043191 (2021).

[54] Sandy Adhitia Ekahana, Y. Soh, Anna Tamai, Daniel Gosálbez-Martínez, Mengyu Yao, Andrew Hunter, Wenhui Fan, Yihao Wang, Junbo Li, Armin Kleibert, C. A. F. Vaz, Junzhang Ma, Hyungjun Lee, Yimin Xiong, Oleg V. Yazyev, Felix Baumberger, Ming Shi, and G. Aeppli, “Anomalous electrons in a metallic kagome ferromagnet,” Nature **627**, 67–72 (2024).

[55] Marcos V. Gonçalves-Faria, Alexej Pashkin, Qi Wang, Hechang C. Lei, Stephan Winnerl, Alexander A. Tsirlin, Manfred Helm, and Ece Uykur, “Coherent phonon and unconventional carriers in the magnetic kagome metal fe_3sn_2 ,” npj Quantum Materials **9** (2024), 10.1038/s41535-024-00642-6.

[56] Wenliang Zhang, Teguh Citra Asmara, Yi Tseng, Junbo Li, Yimin Xiong, Yuan Wei, Tian-

lun Yu, Carlos William Galdino, Zhijia Zhang, Kurt Kummer, Vladimir N. Strocov, Y. Soh, Thorsten Schmitt, and Gabriel Aeppli, “Spin waves and orbital contribution to ferromagnetism in a topological metal,” *Nature Communications* **15** (2024), 10.1038/s41467-024-53152-1.

[57] Lujunyu Wang, Jiaojiao Zhu, Haiyun Chen, Hui Wang, Jinjin Liu, Yue-Xin Huang, Bingyan Jiang, Jiaji Zhao, Hengjie Shi, Guang Tian, Haoyu Wang, Yugui Yao, Dapeng Yu, Zhiwei Wang, Cong Xiao, Shengyuan A. Yang, and Xiaosong Wu, “Orbital Magneto-Nonlinear Anomalous Hall Effect in Kagome Magnet Fe_3Sn_2 ,” *Physical Review Letters* **132**, 106601 (2024).

[58] L A Fenner, A A Dee, and A S Wills, “Non-collinearity and spin frustration in the itinerant kagome ferromagnet Fe_3Sn_2 ,” *Journal of Physics: Condensed Matter* **21**, 452202 (2009).

[59] Bahar Fayyazi, Konstantin P. Skokov, Tom Faske, Ingo Opahle, Michael Duerrschnabel, Tim Helbig, Ivan Soldatov, Urban Rohrmann, Leopoldo Molina-Luna, Konrad Güth, Hongbin Zhang, Wolfgang Donner, Rudolf Schäfer, and Oliver Gutfleisch, “Experimental and computational analysis of binary Fe-Sn ferromagnetic compounds,” *Acta Materialia* **180**, 126–140 (2019).

[60] Kevin Heritage, Ben Bryant, Laura A. Fenner, Andrew S. Wills, Gabriel Aeppli, and Yeong-Ah Soh, “Images of a First-Order Spin-Reorientation Phase Transition in a Metallic Kagome Ferromagnet,” *Advanced Functional Materials* **30** (2020), 10.1002/adfm.201909163.

[61] Peng Wu, Jiuwei Song, Xiaoxiang Yu, Yihao Wang, Kang Xia, Bin Hong, Lin Zu, Yinchang Du, Pierre Vallobra, Fengguang Liu, Shuki Torii, Takashi Kamiyama, Yimin Xiong, and Weisheng Zhao, “Evidence of spin reorientation and anharmonicity in kagome ferromagnet Fe_3Sn_2 ,” *Applied Physics Letters* **119** (2021), 10.1063/5.0063090.

[62] Caihong Xie, Yongcheng Deng, Dong Zhang, Junbo Li, Yimin Xiong, Mangyuan Ma, Fusheng Ma, Wei Tong, Jihao Wang, Wenjie Meng, Yubin Hou, Yuyan Han, Qiyuan Feng, and Qingyou Lu, “Real-Space Imaging of Intrinsic Symmetry-Breaking Spin Textures in a Kagome Lattice,” *Advanced Science* **11** (2024), 10.1002/advs.202404088.

[63] Qi Wang, Shanshan Sun, Xiao Zhang, Fei Pang, and Hechang Lei, “Anomalous Hall effect in a ferromagnetic Fe_3Sn_2 single crystal with a geometrically frustrated Fe bilayer kagome lattice,” *Physical Review B* **94**, 075135 (2016).

[64] Neeraj Kumar, Y. Soh, Yihao Wang, and Y. Xiong, “Magnetotransport as a diagnostic of

spin reorientation: Kagome ferromagnet as a case study,” Physical Review B **100**, 214420 (2019).

[65] Andrew Fitch, Catherine Dejoie, Ezio Covacci, Giorgia Confalonieri, Ola Grendal, Laurent Claustre, Perceval Guillou, Jérôme Kieffer, Wout de Nolf, Sébastien Petitdemange, Marie Ruat, and Yves Watier, “ID22 – the high-resolution powder-diffraction beamline at ESRF,” Journal of Synchrotron Radiation **30**, 1003–1012 (2023).

[66] Alexander A. Tsirlin, Lilian Prodan, and Ola Grendal, “High-resolution x-ray diffraction study of the kagome metal Fe_3Sn_2 ,” European Synchrotron Radiation Facility (2022), 10.15151/ESRF-DC-2007330151.

[67] V. Petříček, M. Dušek, and L. Palatinus, “Crystallographic computing system JANA2006: General features,” Z. Krist. **229**, 345–352 (2014).

[68] U. Stuhr, B. Roessli, S. Gvasaliya, H.M. Rønnow, U. Filges, D. Graf, A. Bollhalder, D. Hohl, R. Bürgi, M. Schild, L. Holitzner, C. Kaegi, P. Keller, and T. Mühlebach, “The thermal triple-axis-spectrometer EIGER at the continuous spallation source SINQ,” Nuclear Instruments and Methods in Physics Research Section A: Accelerators, Spectrometers, Detectors and Associated Equipment **853**, 16–19 (2017).

[69] O. Kazakova, R. Puttock, C. Barton, H. Corte-León, M. Jaafar, V. Neu, and A. Asenjo, “Frontiers of magnetic force microscopy,” Journal of Applied Physics **125** (2019), 10.1063/1.5050712.

[70] Robert C. O’Handley, *Modern Magnetic Materials: Principles and Applications* (Wiley, New York, 1999) p. 184.

[71] B. D. Cullity and C. D. Graham, *Introduction to Magnetic Materials* (Wiley, 2008).

[72] Lilian Prodan, Donald M. Evans, Sinéad M. Griffin, Andreas Östlin, Markus Althaler, Erik Lysne, Irina G. Filippova, Sergiu Shova, Liviu Chioncel, Vladimir Tsurkan, and István Kézsmárki, “Large ordered moment with strong easy-plane anisotropy and vortex-domain pattern in the kagome ferromagnet Fe_3Sn ,” Applied Physics Letters **123** (2023), 10.1063/5.0155295.

[73] Willie Sucksmith and Jo E Thompson, “The magnetic anisotropy of cobalt,” Proceedings of the Royal Society of London. Series A. Mathematical and Physical Sciences **225**, 362–375 (1954).

[74] A. Hubert and R. Schäfer, *Magnetic Domains: The Analysis of Magnetic Microstructures*, Corrected 3rd Printing (Springer, Berlin, Heidelberg, New York, 2009) p. 378.

[75] Yutao Chen, Boyao Lv, Yaodong Wu, Qiyang Hu, Junbo Li, Yihao Wang, Yimin Xiong, Jianhua Gao, Jin Tang, Mingliang Tian, and Haifeng Du, “Effects of tilted magnetocrystalline anisotropy on magnetic domains in Fe_3Sn_2 thin plates,” *Physical Review B* **103**, 214435 (2021).